Biosensors and Bioelectronics 135 (2019) 160–165

Contents lists available at ScienceDirect

Biosensors and Bioelectronics

journal homepage: www.elsevier.com/locate/bios

Photoelectrochemically driven bioconversion and determination of nifedipine based on a double photoelectrode system

Jiuying Tian, Mingjuan Huang, Yanting Yang, Dongyue Wang, Jusheng Lu*

Jiangsu Key Laboratory of Green Synthetic Chemistry for Functional Materials, School of Chemistry and Materials Science, Jiangsu Normal University, Xuzhou, 221116, PR China

ARTICLE INFO

Keywords:
Photoelectrochemically driven
Double photoelectrode
Enzymatic bioconversion and determination
Nifedipine
Cytochrome P450

ABSTRACT

In the present work, a double photoelectrode system has been constructed for photoelectrochemically driven enzymatic bioconversion and determination of nifedipine. In which, the TiO_2 nanotube arrays in-situ assembled with g-C_3N_4 (TNA/g-C_3N_4) was used as a photoanode, and a cytochrome P450 3A4 (CYP3A4) enzyme was immobilized in the porous ITO/CuO films to fabricate an ITO/CuO/CYP3A4 photocathode. The constructed double photoelectrode system had a significant photocurrent response compared to the single ITO/CuO/CYP3A4 or TNA/g-C_3N_4 under visible light irradiation. Under optimal conditions, the photocurrent of the double photoelectrode system had a high catalytic activity toward substrate nifedipine with k_{cat} of 5.62 s^{-1} and catalytic efficiency with k_{cat}/k_m^{app} of 0.94 $\mu M^{-1} s^{-1}$, and the bioconversion yield of nifedipine reached 22.1%. Furthermore, the constructed double photoelectrode system could be used to determine the nifedipine concentration with a high sensitivity of 2.46 $\mu A\ \mu M^{-1}$ and a low detection limit of 0.015 μM. Therefore, the proposed double photoelectrode system can be used well for study enzyme biocatalysis for target bioconversion, and also has a potential application for toxicity analysis.

1. Introduction

Cytochrome P450 enzymes (CYP450s) are a family of heme-containing monooxygenases that can catalyze various regioselective and stereospecific oxygen insertion reactions (Meunier et al., 2004; Denisov et al., 2005; Guengerich, 2008). A typical catalytic process CYP450s is achieved by facilitated by donation of electrons from nicotinamide-adenine dinucleotide phosphate (NADPH) via CYP450 reductase (CPR) to the CYP450's heme center (Krishnan et al., 2011a). There have been some reports of attempts to initiate CYP450 catalysis by replacing the electronic donations of expensive NADPH with electrochemically driven systems (Krishnan et al., 2011b; Mak et al., 2010; Lu et al., 2014; Xu et al., 2012). Different from the electrochemically driven method, the photoelectrochemically driven method, another effectively driven approach in the CYP450 catalysis (Tran et al., 2013; Ipe and Niemeyer, 2006; Xu et al., 2014; Lu et al., 2016), does not require excessive applied potential, thus providing enzymes with a friendly, biocompatible environment to ensure the enzyme with high bioactivity and catalytic properties (Ham et al., 2010; Park et al., 2015).

Inorganic semiconductor nanomaterials are the most popular photoactive materials applied in the photoelectrochemically driven system and can be classified into n-type and p-type, in which, photo-excited electrons are the majority carriers and holes are the minority carriers for n-type semiconductor; whereas, for p-type semiconductor, holes are the majority carriers and electrons are the minority carriers (Hisatomi et al., 2014). Under light irradiation, electrons could be excited from the valence band (VB) of the photoactive material to the conduction band (CB) with the generation of electron-hole pairs. Anodic photocurrent will be generated when the electrode is constructed on n-type photoactive material, which is called a photoanode; cathodic photocurrent will be generated if the electrode is established on p-type photoactive material, which is called a photocathode (Wang et al., 2014; Li et al., 2015a, b; Gill et al., 2008). In the CYP450 catalytic cycle, photocathode can transfer the photo-excited CB electrons to the heme center of CYP450 enzyme in the electrolyte solution, followed by the supply of electrons from the electrode to neutralize the VB holes. Unfortunately, the photocathode uses electrons as the minority carriers and it needs electron acceptor, resulting in very poor photocurrent response and low catalytic efficiency of CYP450 enzyme (Xu et al., 2014; Qian et al., 2014). However, the photoanode uses holes as the minority carriers, and evident photocurrent response can be produced when electron donor exists in the electrolyte solution.

Herein, to play the advantages of photoanode-based nanomaterials, we constructed a novel photoelectrochemically driven CYP450

* Corresponding author. School of Chemistry and Materials Science, Jiangsu Normal University, 101 Shanghai Road, Xuzhou, 221116, PR China.
E-mail address: jushenglu@jsnu.edu.cn (J. Lu).

https://doi.org/10.1016/j.bios.2019.04.020
Received 19 February 2019; Received in revised form 30 March 2019; Accepted 10 April 2019
Available online 16 April 2019
0956-5663/ © 2019 Elsevier B.V. All rights reserved.

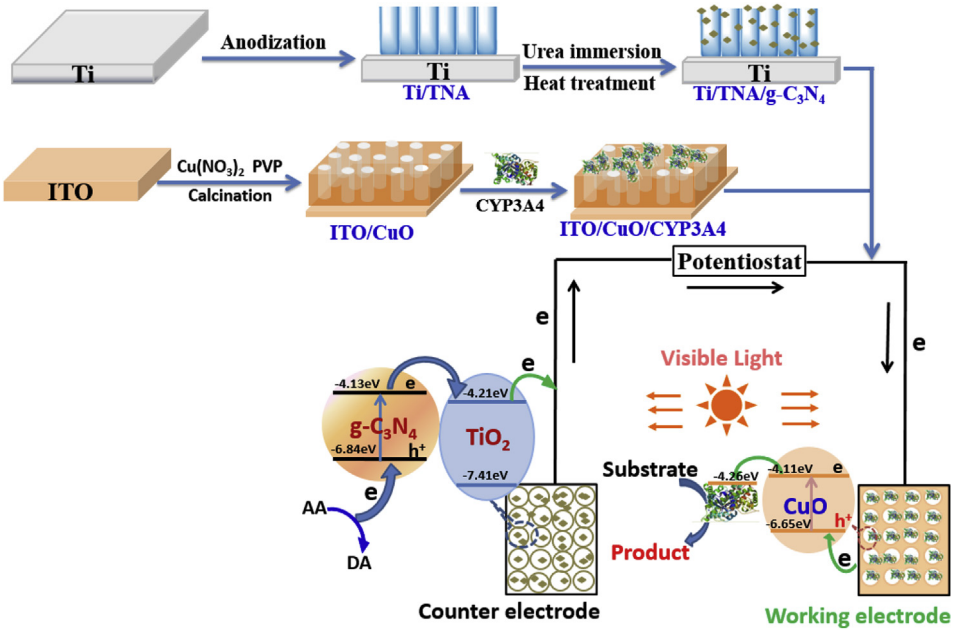

Scheme 1. Construction of the double photoelectrode system for photoelectrochemically driven enzymatic bioconversion and determination of target.

enzymatic platform based on a double photoelectrode system containing both an ITO/CuO/CYP3A4 photocathode and a TNA/g-C_3N_4 photoanode. As illustrated in Scheme 1, the fabricated ITO/CuO/CYP3A4 photocathode and TNA/g-C_3N_4 photoanode were used as a working electrode and a counter electrode, respectively. Under the visible light irradiation, excited electrons transferred from the CB of g-C_3N_4 to that of TNAs and transferred to the photocathode through the external circuit, which would effectively increase the photocurrent and provide sufficient electrons for the CYP3A4 enzymatic bioconversion of the substrate. At the same time, the enzymatic platform could also be used for the determination of targets. Therefore, a double photoelectrode system for photoelectrochemically driven enzymatic bioconversion and determination of substrate would be successfully constructed.

2. Experimental

2.1. Materials and reagents

Titanium foils (99.7% purity) with a thickness of 0.127 mm, nifedipine, CYP3A4 enzyme and urea were purchased from Sigma-Aldrich Co. Ltd. (St. Louis, MO, USA). Polyvinylpyrrolidone (PVP, K90, 6.3×10^5 in viscosity average molecular weight), $Cu(NO_3)_2.3H_2O$, glycerol, and NH_4F were obtained from Sinopharm Chemical Reagent Co. Ltd. (Shanghai, China). Phosphate buffer solution (PBS, 10 mM, pH 7.4) was prepared by mixing the stock solution of K_2HPO_4 and KH_2PO_4. All other chemicals were of at least analytical grade and used as received. Deionized water (18.2 MΩ cm) obtained from a Milli-Q water purification system was used in all measurements.

2.2. Apparatus

The morphology of all nanomaterials was characterized by Hitachi S-4800 scanning electron microscope (Japan) and JEM-2100 transmission electron microscope (JEOL, Japan), respectively. The crystal structures of nanomaterials were identified by X-ray diffraction (XRD) with Philips X'Pert Pro diffractometer by Ni-filtered Cu Kα radiation (λ = 0.154178 nm). UV–vis absorption spectra were measured on a UV-2450 spectrometer (Shimadzu, Japan). Liquid chromatography (LC) analyses for nifedipine and its metabolite were performed using an Agilent series 1200 high performance liquid chromatography (HPLC) system (Agilent, Palo Alto, CA). A solution of 10 μL of sample was injected into a 4.6 mm × 150 mm Zorbax Eclipse 5 μm XDB-C18 reverse-phase column. The separation was performed using a mobile phase of water and ethanol (75:25, v/v) at a flow rate of 0.5 mL min^{-1} with UV detection wavelength at 360 nm.

2.3. Fabrication of TNA/g-C_3N_4 photoanode

The TiO_2 nanotube arrays (TNAs) on titanium foil were fabricated by the electrochemical anodization technique according to our previous work (Lu et al., 2014), which were thoroughly rinsed and immersed in urea solution (10 wt%) for 4 h. Then, the TNAs absorbed with urea were directly heated to 550 °C at a rate of 2 °C min^{-1} and then kept at this temperature for another 3 h in a in a muffle furnace to prepare a TNA/g-C_3N_4 photoanode nanomaterial.

2.4. Fabrication of ITO/CuO/CYP3A4 photocathode

2.0 g of PVP and 4.5 g of $Cu(NO_3)_2$ were added and dissolved in 40 mL water under stirring at room temperature, then the mixed solution was deposited on the ITO glass substrates (20 mm × 40 mm × 1.0 mm) by dip-coating, where the ITO slides were withdrawn at 2 cm min^{-1}. Then the gel films were directly transferred into a muffle furnace held at 500 °C in an air atmosphere for 20 min, and the dip coating and calcination of gel films were repeated 3 times. Then the resultant ITO/CuO were immersed in 1.0 μM CYP3A4 solution in 10 mM PBS (pH 7.4) at 4 °C for 24 h with gentle stirring. The enzyme-modified ITO/CuO (ITO/CuO/CYP3A4) were then rinsed and stored in 10 mM PBS (pH 7.4) at 4 °C until use.

2.5. Construction of a photoelectrochemically-driven enzymatic platform based on the double photoelectrode system

Photoelectrochemically-driven enzymatic bioconversion and determination of substrate was carried out on a CHI660E electrochemical workstation (CH Instruments, Austin, USA), in which, a conventional three-electrode system composing of an ITO/CuO/CYP3A4 photocathode as the working electrode, a TNA/g-C_3N_4 photoanode as the counter electrode and a saturated calomel electrode (SCE) as the reference electrode, respectively. A 500 W Xe lamp was used as an

irradiation source fitted with a 400 nm UV filter (Zolix, China) and a mechanical shutter was used to make the light on and off. The reaction medium solution was an air-saturated PBS (0.1 M, pH 7.4) solution containing 0.1 M of ascorbic acid (AA) and different amounts of nifedipine. After visible light irradiation, the determination of nifedipine was carried out according to the photocurrent change of the double photoelectrode system, and the bioconversion of nifedipine was monitored by liquid chromatography.

3. Results and discussion

3.1. Fabrication of TNA/g-C_3N_4 photoanode and ITO/CuO/CYP3A4 photocathode

As an inorganic semiconductor, vertically aligned TNAs have been applied in the photoelectrochemical sensors due to its large interior and outer surface area, photochemical stability, good biocompatibility and chemical stability (Zhang et al., 2008; Li et al., 2015a, b). Nevertheless, TiO_2 has a wide band gap and cannot be excited by visible light (Tachikawa et al., 2011; Chen and Mao, 2007), limiting its PEC applications for biomolecules. Graphitic carbon nitride (g-C_3N_4) is a good photoactive semiconductor under visible light irradiation due to its moderate band gap (~2.7 eV) (Cao and Yu, 2014), which possesses high chemical and thermal stability as well as fascinating electronic property (Hu et al., 2014). In the present work, TNAs were fabricated by electrochemical anodization (Fig. 1A). After immersing in the 10 wt % urea solution for 4 h and calcination at 550 °C for 3 h, some g-C_3N_4 were distributed on the surface of TNAs from the SEM images (Fig. 1 B), which had a graphitic-like nanosheet structure as shown in the TEM image (Inset of Fig. 1 B). The energy dispersive spectroscopy (EDS) showed the existence of C, N, Ti and O, confirming the in-situ growth of g-C_3N_4 on TNAs (Fig. 1 C). Furthermore, X-Ray diffraction (XRD) patterns (Fig. 1 D) showed that, for pure g-C_3N_4 (curve c of Fig. 1D), two peaks at 13.0° and 27.4° were corresponding to the (100) and (002) crystal planes, respectively (JCPDS 87–1526) (Lee et al., 2012; Liao et al., 2012). However, the peak of g-C_3N_4 at 13.0° was absent in TNA/g-C_3N_4, while only a small peak at 27.4° was observed (curve d of Fig. 1D), most likely due to the low percentage composition of g-C_3N_4 in the TNA/g-C_3N_4.

For fabrication of the photocathode, a porous CuO films on ITO slide was prepared by dip coating and calcination. The results showed that, it was easy to form a porous CuO film on ITO in the presence of PVP. When the molar ratio of PVP to Cu^{2+} was 2: 5, the prepared CuO nanoparticles had an average size of 80 nm, the pores formed were uniformly distributed on the film (Fig. 1E), and the thickness of the film was about 200 nm from the SEM cross section image (Fig. S1). From XRD patterns (Fig. 1 F), the peaks at 32.5°, 35.6°, 38.7°, 48.9°, 53.5°, 58.3°, 61.5°, 66.2°, 68.1°, 72.4° and 75.2° were indexed to (110), (−111), (111), (−202), (020), (202), (−113), (−311), (220), (311) and (−222) respectively (JCPDS 80–1916), suggesting the formation of CuO on the surface of ITO slide (Kim et al., 2016).

3.2. Photoelectrochemical response of different systems

Under visible light irradiation, no significant photocurrent was observed for TNAs, however a typically anodic photocurrent could be observed for TNA/g-C_3N_4 (Curve a and b of Fig. 2A). It was because that, the CB and VB of TNAs were located at −4.21 and −7.41 eV, respectively, and the band gap energy of TNAs was 3.2 eV, which could not be excited under visible light irradiation (Tachikawa et al., 2011). g-C_3N_4 had a band gap energy of 2.71 eV determined by UV–vis absorption spectrum (Fig. S2A and inset), and the CB and VB positions were quantified at −4.13 eV and −6.84 eV, respectively coupled with the formal redox potential peak at −0.61 V (vs. SCE, Fig. S2B). Under visible light irradiation, the electrons could excite from the VB to CB of g-C_3N_4, then quickly transferred to the CB of TNAs due to the more positive CB of TNAs, resulting in the increasing photocurrent. Furthermore, the as-prepared TNA/g-C_3N_4 had good photostability, no more than 3.0% of the initial photocurrents decreased after 20 cycles of repeated light irradiation (Fig. S3), which was important for the construction of a photoelectrochemical driven system.

On the other hand, when the ITO/CuO served as working electrode, a photocathode current was observed under visible light irradiation (curve c of Fig. 2A). After assemble CYP3A4 enzyme on the ITO/CuO to construct an ITO/CuO/CYP3A4 phocathode, the photocurrent further increased (curve d of Fig. 2A). It was due that, the CB and VB positions of CuO was calculated at −4.11 eV and −6.65 eV respectively by the UV–vis absorption spectrum and cyclic voltammogram (Fig. S4 A and B), the energy level of CYP3A4 of −4.26 eV was calculated according to its formal redox potential at −0.48 V (vs. SCE) (Huang et al., 2012), which lied between the CB and VB positions of CuO, providing the possibility of allowing fast electron injection from the excited CuO to the heme of CYP3A4. However, the overall photocurrent was still relatively small due to the p-type semiconductor of CuO with electrons as

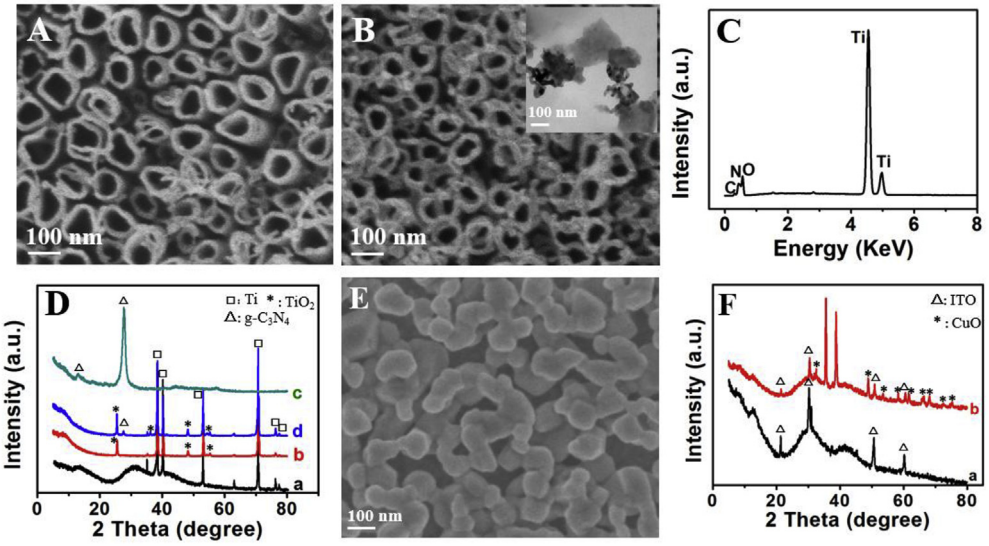

Fig. 1. SEM image of TNA (A) and TNA/g-C_3N_4 (B), Inset: TEM image of g-C_3N_4. (C) EDS of TNA/g-C_3N_4. (D) XRD pattern of Ti substrate (a), TNA (b), g-C_3N_4 (c) and TNA/g-C_3N_4 (d). (E) SEM image of ITO/CuO. (F) XRD patterns of ITO (a) and ITO/CuO (b).

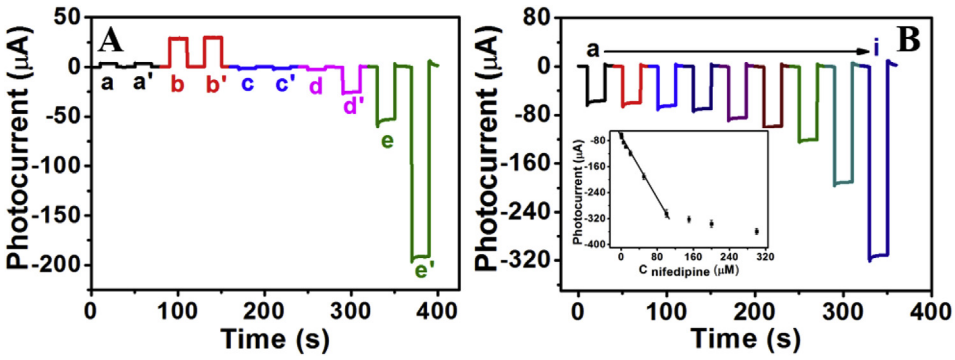

Fig. 2. (A) Photocurrent response of TNA (a, a'), TNA/g-C_3N_4 (b, b'), ITO/CuO (c, c'), ITO/CuO/CYP3A4 (d, d'), the double photoelectrode system (e, e') before (a, b, c, d, e) or after (a', b', c', d', e') adding 50 μM of nifedipine. (B) Photocurrent response of the double photoelectrode system after adding nifedipine with the concentration of 0.05–100 μM (a–i), Inset: Calibration curve of the photocurrent of the double photoelectrode system versus the concentration of nifedipine. Applied potential, 0 V.

the minority carriers.

Furthermore, when ITO/CuO/CYP3A4 was used as working electrode, and TNA/g-C_3N_4 was used as the counter electrode respectively to form a double photoelectrode system (Scheme 1), holes on the VB of ITO/CuO/CYP3A4 significantly attracted photo-excited electron of the TNA/g-C_3N_4, resulting in ultra-fast electron transfer from the TNA/g-C_3N_4 to the ITO/CuO through the external circuit, the photocurrent response of the system would increase significantly (Curve e of Fig. 2A) (Xin et al., 2011; Wu et al., 2012). Nifedipine, a nitroarene drug clinically used for the treatment of high blood pressure, cardiovascular disease, angina pectoris and migraine after oral eat (Weiss, 1991), could be bioconversed to dehydronifedipine by CYP3A4 catalysis (Racha et al., 2003). After the addition of 50 μM of nifedipine, no significant changes were observed in photocurrent for TNA, TNA/g-C_3N_4 or ITO/CuO system (Curve a', b' or c' of Fig. 2A). For ITO/CuO/CYP3A4 system, the photocurrent response had a certain increase after adding nifedipine (curve d' of Fig. 2A), however it was significantly smaller than that of the double photoelectrode system (curve e' of Fig. 2A). In addition, when the CYP3A4 enzyme was not assemble on the ITO/CuO, the photocurrent response of the double photoelectrode system did not change significantly before and after adding nifedipine (Fig. S5). Therefore, all of these suggested the successful enzymatic bioconversion of nifedipine driven by the double photoelectrode system, which consumed the electrons generated from the excited state of CuO to the hemo center of CYP3A4 for the enzymatic bioconversion of nifedipine.

3.3. Effect of morphology of the TNA/g-C_3N_4 and CuO on the enzymatic bioconversion performance of nifedipine

As an electron donor, the performance of TNA/g-C_3N_4 had a great effect on the photocurrent response of the double photoelectrode system and the bioconversion of nifedipine. When TNAs were fabricated by electrochemical anodization at an anodization time of 4 h and with different anodization potential from 10 V to 30 V, the inner diameters increased from about 25 nm to 200 nm in sequence (Fig. 3). After immersing in urea solution and then calcination, for the TNAs with small inner diameters, the generated g-C_3N_4 almost accumulated on the surface of the TNA (Fig. 3A and B), which resulted in the low photocurrent of the double-photoelectrode system (Curve a and b of Fig. 3F). It may be due to that, the small tubes made it difficult for urea to enter the tubes of TNAs, causing a large amount of g-C_3N_4 accumulate on the TNA's surface, hindering the transfer of photo-excited electrons to the electrode. In addition, due to the relatively large inner diameter of TNAs as shown in Fig. 3E, g-C_3N_4 was difficult to generate in situ on the surface of TNAs, leading to the lower photocurrent of the system (Curve e of Fig. 3F). Only when the TNAs had an inner diameter of ~100 nm (Fig. 3C), or ~150 nm (Fig. 3D), the generated g-C_3N_4 could be uniformly distributed on the surface of TNAs and the photocurrent responses of the double-photoelectrode system were relatively significant (Curve c and d of Fig. 3F). Therefore, the TNA anodized with potentials of 20 V for 4 h was used in the experiment.

Furthermore, when the obtained CuO film was a single layer (Fig. 4A), the assembled CYP3A4 was in a relatively open environment, resulting in the low enzyme affinity to substrate (K_m^{app}, 32.4 μM), and small enzymatic rate constant k_{cat} with 0.61 s^{-1} (Fig. 4 E and F). In addition, the CuO films obtained by dip coating for 3 times had a multi-layered porous structure with the thickness of about 200 nm (Fig. 4 B-D and Fig. S1). When the molar ratios of Cu^{2+} and PVP was 5:1, the obtained CuO film was relatively dense, and no obvious pores were observed (Fig. 4B), or the molar ratios of Cu^{2+} and PVP was 5:3, the pores between the CuO nanoparticles on the films were relatively large, the assembled CYP3A4 was all in a relatively open environment, the enzyme affinity to substrate and the enzymatic activity were all relatively low with K_m^{app} of 25.6 μM, 12.4 μM and k_{cat} of 1.15 s^{-1}, 2.49 s^{-1}, respectively (Fig. 4 E and F). Only when the molar ratios of Cu^{2+} and PVP of 5:2, the produced CuO film had an average distribution of pores of about 100 nm. When the CYP3A4 enzyme was confined in such films with suitable pore diameters (confined spaces) that had a size similar to itself, the confinement effect facilitated the maintenance of bioactivity and the high affinity to substrate of immobilized enzyme (Chen et al., 2009), the enzymatic activity and catalytic efficiency of CYP3A4 toward nifedipine were the highest, k_{cat} and k_{cat}/K_m^{app} were 5.62 s^{-1} and 0.94 $\mu M^{-1} s^{-1}$, respectively (Fig. 4 E and F), which were remarkably better than the values reported in previous literature (Niwa et al., 2008; Uehara et al., 2017; Jiang et al., 2011).

3.4. Optimization of experimental conditions on the determination of nifedipine

Based on the above preferred photocathode and photoanode nanomaterials, the double photoelectrode system could be used for the determination of nifedipine. To achieve optimal photocurrent response, several experimental parameters including the concentration of ascorbic acid, intensity of visible light irradiation, calcination time of CuO film and medium pH were investigated for the 50 μM of nifedipine (Fig. S6). The concentration of ascorbic acid had a greater impact on the photocurrent of the system because it served as an electron donor for generation of photocurrent, the photocurrent was enhanced with the increasing of ascorbic acid concentration up to 0.1 M, and then almost unchanged with further addition of ascorbic acid (Fig. S6A). Thus, 0.1 M of ascorbic acid was selected for the next experiments. Similarly, the intensity of visible light irradiation played an important role in PEC biosensing since the light intensity affects the generation of photo-excited electrons/holes. As shown in Fig. S6B, the photocurrent increased with the increase of irradiation intensity, and tended to be stable after 200 mW cm^{-2}. In addition, the calcination time of CuO film was investigated, when the calcination time was 20 min, the photocurrent of the system reached the maximum (Fig. S6C), which may be because the shorter time is not conducive to the decomposition and dissipation of PVP. Furthermore, the medium pH affects the activity of CYP3A4 enzyme. The results showed that (Fig. S6D), the photocurrent response increased at first with increasing pH of solution, the maximum response

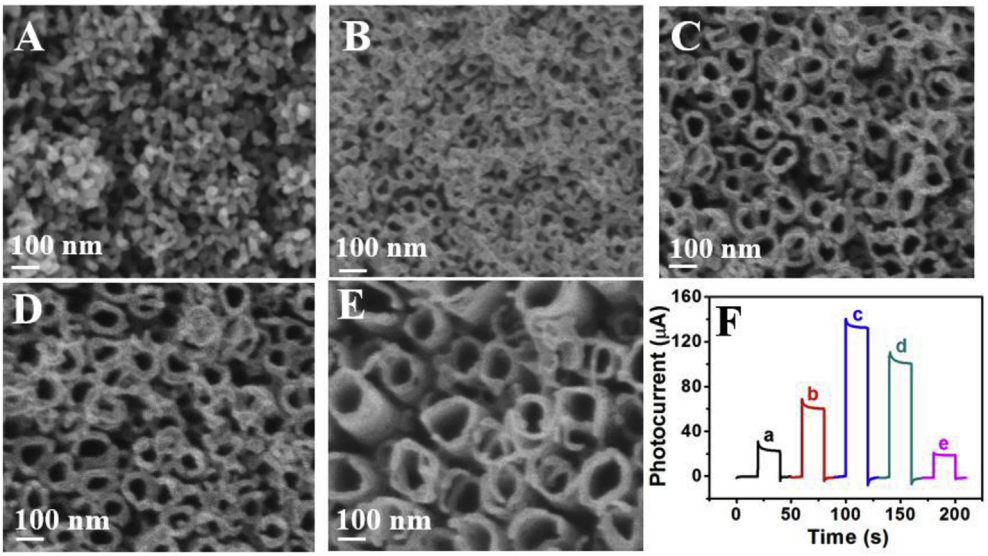

Fig. 3. SEM images (A–E) of TNA/g-C_3N_4 with 4 h of anodization time and different anodization potentials of 10 V (A), 15 V (B), 20 V (C), 25 V (D) and 30 V (E). (F) Corresponding photocurrent responses of TNA/g-C_3N_4 with different anodization potentials of 10 V (a), 15 V (b), 20 V (c), 25 V (d) and 30 V (e).

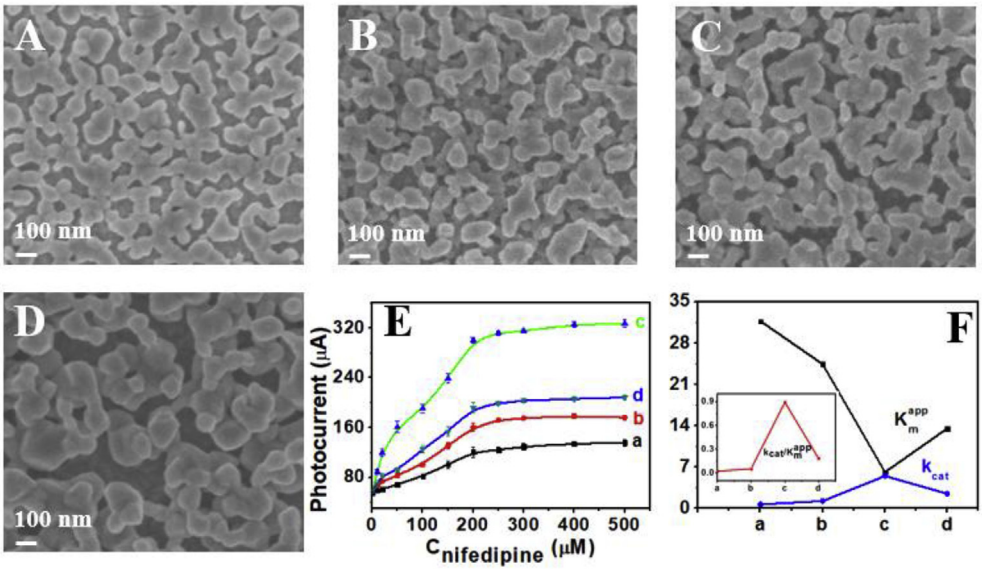

Fig. 4. SEM images of single-layer CuO films (A) and multi-layer CuO films prepared with molar ratio of Cu^{2+} and PVP of 5:1 (B), 5:2 (C), or 5:3 (D). (E) Corresponding Michaelis – Menten plots, and (F) kinetic parameters of ITO/CuO/CYP3A4 with single layer (a), and molar ratio of Cu^{2+} and PVP of 5:1 (b), 5:2 (c), or 5:3 (d), respectively.

was obtained at pH 7.5. But the photocurrent decreased when the pH was larger than 8.0. So, 0.1 M PBS solution with pH 7.4, a physiological pH value, was used in the experiments.

3.5. Enzymatic determination of nifedipine by the double photoelectrode system

Based on the above preferred photocathode and photoanode nanomaterials, the double photoelectrode system could be used for the determination of nifedipine. As shown in Fig. 2B, with the continuous addition of nifedipine solution, the photocurrent increased, and the increased value was linear with the concentration of nifedipine in the range of 0.05–100 μM (Inset of Fig. 2B), the linear fitting equation was $I = -2.46c - 66.54$, and the limit of detection (LOD) was 0.015 μM at a signal-to-noise ratio of 3. From the slope of 2.46, the sensitivity of the system to nifedipine determination was 2.46 μA μM^{-1}, providing the possibility for quantitative determination of nifedipine by the proposed double photoelectrode system. Compared to other reported analytical methods in Table 1, the proposed assay for nifedipine determination exhibited an ideal measurement range and high sensitivity. Meanwhile, the system can also be extended to the application of the determination of other substrates.

As a biosensor for nifedipine determination, the reproducibility of the double photoelectrode system was studied, the relative standard deviation (RSD) was evaluated to be 4.2% by 10 successive measurements for a single biosensor, and the RSD was calculated to be 7.5% for 6 biosensors, which indicated good reproducibility of the double photoelectrode system as a biosensor. Moreover, the double photoelectrode system had a good operational stability and the photocurrent did not change significantly for determination 5.0 μM of nifedipine at regular intervals of every other day after 15 days' storage in 0.1 M pH 7.4 PBS at 4 °C.

3.6. Enzymatic bioconversion of nifedipine by the double photoelectrode system

The photoelectrochemically-driven enzymatic bioconversion of nifedipine with the double photoelectrode system could be identified by the high-performance liquid chromatography (HPLC). After visible light irradiation for 2 h, the liquid chromatogram of the nifedipine solution

Table 1
Comparison of the proposed method for nifedipine determination with other previously reported works.

Methods	Linear range (μM)	LOD (μM)	Reference
Voltammetry	0.2–104.41	0.032	Khairy et al. (2017)
Chromatography	0.58–28.88	0.17	Ahmed et al. (2018)
MIT fluorometry	0.28–3.4	0.076	Jalili and Amjadi (2015)
Capillary electrophoresis	2.89–144.38	0.31	Zeng et al. (2015)
Spectrofluorometry	0.58–11.55	0.049	Al-Ghannam and Al-Olyan (2008)
Electrochemistry	0.8–60.0	0.72	Baghayeri et al. (2013)
PEC sensor	0.25–18.0	0.15	Peng et al. (2019)
UPLC	0.72–4.33	0.14	Galan-Rodriguez et al. (2015)
Double photoelectrode PEC	0.05–100	0.015	This work

showed two peaks at 4.12 and 6.27 min (Fig. S7B), while only one peak at 6.27 min was observed for the pure nifedipine (Fig. S7A). So the peak at 6.27 min was attributed to the metabolite of dehydronifedipine, which increased the polarity of nifedipine. However, in the absence of visible light irradiation, no dehydronifedipine was produced (Fig. S8), which further demonstrated that the bioconversion of nifedipine was driven by photoelectrochemistry with the double photoelectrode system. The bioconversion yields of dehydronifedipine for different CuO films, calculated by dividing the LC peak area at 4.12 min by total LC peak area of 6.27 and 4.12 min, increased with the increase of the time of visible light irradiation (Fig. S8), and could reach to 22.1% for CuO film with molar ratios of Cu^{2+} and PVP of 5:2 with visible light irradiation for 2 h (Fig. S7B), which was significantly higher than that of the previous reported literature (Huang et al., 2012). However, the bioconversion yields of nifedipine were all relatively low, whether for CuO prepared with molar ratios of Cu^{2+} and PVP of 5:1 or 5:3, which was only 4.2% and 8.9%, respectively (Fig. S7 C and D), further indicating that CYP3A4 spatially confined in the pores of CuO film could exhibit excellent enzymatic activity and catalytic efficiency. In addition.

4. Conclusions

In summary, a novel photoelectrochemically driven enzymatic platform was constructed for substrate nifedipine bioconversion and determination based on a double photoelectrode system containing both an ITO/CuO/CYP3A4 photocathode and a TNA/g-C_3N_4 photoanode. By optimizing the experimental conditions, the double photoelectrode system had a high enzymatic efficiency for the bioconversion of nifedipine with k_{cat} of 5.62 s^{-1} and k_{cat}/k_m^{app} of 0.94 $\mu M^{-1} s^{-1}$, and the bioconversion yield of nifedipine reached 22.1% with visible light irradiation for 2 h. And the double photoelectrode system could also be a sensitive biosensor for the determination of nifedipine with a low LOD of 0.015 μM and a wide linear range from 0.05 to 100 μM, which can further be expanded to other CYP450 enzymes for applications in drug discovery and development by monitoring substrate bioconversion.

CRediT authorship contribution statement

Jiuying Tian: Conceptualization, Methodology, Data curation, Writing - original draft. **Mingjuan Huang:** Investigation, Methodology. **Yanting Yang:** Methodology. **Dongyue Wang:** Data curation, Writing - review & editing. **Jusheng Lu:** Conceptualization, Writing - review & editing, Project administration.

Acknowledgements

We gratefully appreciate the financial support from the Top-notch Academic Programs Project of Jiangsu Higher Education Institutions (TAPP), the Science and Technology Project of Xuzhou City (KH17027) and the Undergraduate Students Project of Jiangsu Province (201810320032Z).

Appendix A. Supplementary data

Supplementary data to this article can be found online at https://doi.org/10.1016/j.bios.2019.04.020.

References

Ahmed, S., Alqurshi, A., Mohamed, A.I., 2018. Talanta 184, 296–306.
Al-Ghannam, S.M., Al-Olyan, A.M., 2008. Cent. Eur. J. Chem. 6, 222–228.
Baghayeri, M., Namadchian, M., Karimi-Maleh, H., Beitollahi, H., 2013. J. Electroanal. Chem. 697, 53–59.
Cao, S.W., Yu, J.G., 2014. J. Phys. Chem. Lett. 5, 2101–2107.
Chen, Q., Schonherr, H., Vancso, G.J., 2009. Small 5, 1436–1445.
Chen, X., Mao, S.S., 2007. Chem. Rev. 107, 2891–2959.
Denisov, I.G., Makris, T.M., Sligar, S.G., Schlichting, I., 2005. Chem. Rev. 105, 2253–2277.
Galan-Rodriguez, C., Gonzalez-Alvarez, J., Valls-Remoli, M., 2015. Biomed. Chromatogr. 29, 233–239.
Gill, R., Zayats, M., Willner, I., 2008. Angew. Chem. Int. Ed. 47, 7602–7625.
Guengerich, F.P., 2008. Chem. Res. Toxicol. 21, 70–83.
Ham, M.H., Choi, J.H., Boghossian, A.A., Jeng, E.S., Graff, R.A., Heller, D.A., Chang, A.C., Mattis, A., Bayburt, T.H., Grinkova, Y.V., Zeiger, A.S., Van Vliet, K.J., Hobbie, E.K., Sligar, S.G., Wraight, C.A., Strano, M.S., 2010. Nat. Chem. 2, 929–936.
Hisatomi, T., Kubota, J., Domen, K., 2014. Chem. Soc. Rev. 43, 7520–7535.
Hu, S.Z., Ma, L., You, J.G., Li, F.Y., Fan, Z.P., Lu, G., Liu, D., Gui, J.Z., 2014. Appl. Surf. Sci. 311, 164–171.
Huang, M.H., Xu, X., Yang, H., Liu, S.Q., 2012. RSC Adv. 2, 12844–12850.
Ipe, B.I., Niemeyer, C.M., 2006. Angew. Chem. Int. Ed. 45, 504–507.
Jalili, R., Amjadi, M., 2015. RSC Adv. 5, 74084–74090.
Jiang, J., Wang, J.P., Cai, H., Li, K.B., Deng, Y.Q., 2011. Catal. Commun. 12, 694–697.
Khairy, M., Khorshed, A.A., Rashwan, F.A., Salah, G.A., Abdel-Wadood, H.M., Banks, C.E., 2017. Sensor. Actuator. B Chem. 252, 1045–1054.
Kim, H.S., Kumar, M.D., Patel, M., Kim, J., 2016. Sens. Actuators, A 252, 35–41.
Krishnan, S., Schenkman, J.B., Rusling, J.F., 2011a. J. Phys. Chem. B 115, 8371–8380.
Krishnan, S., Wasalathanthri, D., Zhao, L.L., Schenkman, J.B., Rusling, J.F., 2011b. J. Am. Chem. Soc. 133, 1459–1465.
Lee, S.C., Lintang, H.O., Yuliati, L., 2012. Chem. Asian J. 7, 2139–2144.
Li, H., Xing, J.H., Xia, Z.B., Chen, J.Q., 2015a. Carbon 81, 474–487.
Li, Z.Z., Xin, Y.M., Zhang, Z.H., 2015b. Anal. Chem. 87, 10491–10497.
Liao, G.Z., Chen, S., Quan, X., Yu, H.T., Zhao, H.M., 2012. J. Mater. Chem. 22, 2721–2726.
Lu, J.S., Li, H.N., Cui, D.M., Zhang, Y.J., Liu, S.Q., 2014. Anal. Chem. 86, 8003–8009.
Lu, J.S., Shen, Y.F., Liu, S.Q., 2016. Chem. Commun. 52, 7703–7706.
Mak, L.H., Sadeghi, S.J., Fantuzzi, A., Gilardi, G., 2010. Anal. Chem. 82, 5357–5362.
Meunier, B., de Visser, S.P., Shaik, S., 2004. Chem. Rev. 104, 3947–3980.
Niwa, T., Shiraga, T., Yamasaki, S., Ishibashi, K., Ohno, Y., Kagayama, A., 2008. Xenobiotica 33, 717–729.
Park, J.H., Lee, S.H., Cha, G.S., Choi, D.S., Nam, D.H., Lee, J.H., Lee, J.K., Yun, C.H., Jeong, K.J., Park, C.B., 2015. Angew. Chem. Int. Ed. 54, 969–973.
Peng, J.Y., Zhuge, W.F., Huang, Y.Y., Zhang, C.Z., Huang, W., 2019. Bull. Korean Chem. Soc. 40, 214–219.
Qian, J., Zhu, W., Mi, L., Xu, X., Yu, J.C., Cui, D.M., Xue, Y.C., Liu, S.Q., 2014. J. Electroanal. Chem. 733, 27–32.
Racha, J.K., Zhao, Z.S., Olejnik, N., Warner, N., Chan, R., Moore, D., Satoh, H., 2003. Drug Metab. Pharmacokinet. 18, 128–138.
Tachikawa, T., Yamashita, S., Majima, T., 2011. J. Am. Chem. Soc. 133, 7197–7204.
Tran, N.H., Nguyen, D., Dwaraknath, S., Mahadevan, S., Chavez, G., Nguyen, A., Dao, T., Mullen, S., Nguyen, T.A., Cheruzel, L.E., 2013. J. Am. Chem. Soc. 135, 14484–14487.
Uehara, S., Uno, Y., Nakanishi, K., Ishii, S., Inoue, T., Sasaki, E., Yamazaki, H., 2017. Drug Metab. Dispos. 45, 457–467.
Wang, G.L., Liu, K.L., Dong, Y.M., Wu, X.M., Li, Z.J., Zhang, C., 2014. Biosens. Bioelectron. 62, 66–72.
Weiss, R.J., 1991. Am. Fam. Physician 44, 2075–2082.
Wu, M., Lin, X., Wang, Y., Wang, L., Guo, W., Qi, D., Peng, X., Hagfeldt, A., Gratzel, M., Ma, T., 2012. J. Am. Chem. Soc. 134, 3419–3428.
Xin, X.K., He, M., Han, W., Jung, J., Lin, Z.Q., 2011. Angew. Chem. Int. Ed. 50, 11739–11742.
Xu, X., Wei, W., Huang, M.H., Yao, L., Liu, S.Q., 2012. Chem. Commun. 48, 7802–7804.
Xu, X., Qian, J., Yu, J.C., Zhang, Y.J., Liu, S.Q., 2014. Chem. Commun. 50, 7607–7610.
Zeng, L., Wu, X., Li, Y.X., Lu, D., Sun, C.J., 2015. Anal. Methods 7, 543–550.
Zhang, H., Wang, G., Chen, D., Lv, X.J., Li, J.H., 2008. Chem. Mater. 20, 6543–6549.